Available online at www.sciencedirect.com

ScienceDirect

journal homepage: http://www.elsevier.com/locate/acme

Original Research Article

Study on the post-rolling direction of severely plastic deformed Aluminum-Manganese-Silicon alloy

Mohammad Reza Jandaghi [a,*], *Hesam Pouraliakbar* [b], *Gholamreza Khalaj* [a], *Mohammad-Javad Khalaj* [a], *Akbar Heidarzadeh* [c]

[a] *Young Researchers and Elites Club, Saveh Branch, Islamic Azad University, Saveh, Iran*
[b] *Department of Advanced Materials, WorldTech Scientific Research Center (WT-SRC), Tehran, Iran*
[c] *Department of Materials Engineering, Azarbaijan Shahid Madani University, Tabriz, Iran*

ARTICLE INFO

Article history:
Received 30 November 2015
Accepted 19 June 2016
Available online 14 July 2016

Keywords:
CGP
Post-rolling
XRD
Microstructure
Mechanical properties

ABSTRACT

Constrained groove pressing (CGP) as a severe plastic deformation (SPD) technique was applied on Al-Mn-Si sheets. In the following, direct- and cross-rolling were employed as supplementary processing in order to investigate the rolling-direction effect on CGPed sheets. The in-depth characterization of microstructural evolutions were employed using polarized light microscope and scanning electron microscope. Williamson–Hall analysis method was applied on X-ray diffraction (XRD) patterns of specimens. Analysis of XRD results revealed that post-rolling of CGPed sheets induced dynamic recrystallization (DRX) due to massive dislocations' accumulation which follows by crystallite growth. The largest crystallite size which was 619 nm achieved after direct-rolling through the rolling strain of 1.27. Maximum acquired peak intensity ratio for rolled sheets was for (220) crystallographic plane similar to annealed one. Also, post-rolling had altered the distinguished plane from (111) for CGPed sheets into (220). Mechanical characteristics of specimens were examined using hardness and tension tests. Based on the obtained results, direct-rolling of CGPed samples was more susceptible for strength enhancement compared to cross-rolling. Optimum achieved values for yield and ultimate tensile strength were 155 and 197 MPa, respectively. Rolling in the both longitudinal and cross directions had almost similar effect on the final attained hardness.

* *Corresponding author*. Tel.: +98 912 7325658.
E-mail address: mrj.sharif86@gmail.com (M.R. Jandaghi).
http://dx.doi.org/10.1016/j.acme.2016.06.005

1. Introduction

Ultra-fine grained (UFG) materials have got significant attraction in recent years since they have had unique combination of physical and mechanical properties compared to those of coarse-grained [1]. Approaching to nanostructure have remarkable effect on mechanical strength enhancement; especially in the case of light metals such as aluminum alloys whereby the grain refinement lead to ennoblement of the strength to weight ratio and makes them susceptible more than ever to be employed in transportation and aerospace industries [2]. For this purpose, different SPD methods such as, equal channel angular pressing (ECAP) [3], high pressure torsion (HPT) [4], accumulative back extrusion (ABE) [5], tubular channel angular pressing (TCAP) [6], accumulative roll bonding (ARB) [7], repetitive corrugation and straightening (RCS) [8], multi directional forging (MDF) [9] have been investigated broadly in the recent years. However, some of the mentioned techniques practically ineffectual for the manufacturing of plate-shaped products. ARB and CGP are two versatile SPD techniques for consolidation of metallic sheets. CGP induces the repetitive shear deformation under plane-strain condition utilizing the successive pressings with asymmetric grooved and flattened dies [10]. More details on CGP could be found in literature [10,11].

Cold rolling is known as one of the most advantageous metal working processes for continuous production of bulky materials having shapes such as plate, sheet and bar. Literature claims suggest that the rolled structures usually have lamellar structure with low-angle grain boundaries while the ultra-fine grained structures owing to severe straining are often granular-type containing mainly high-angle grain boundaries [12]. Also, more recent works [13–15] highlighted that further rolling of severely deformed samples spread the high-angle boundaries within the structure resulted in uniform ultra-fine grained material achievement. Hansen et al. [16–18] provided a thorough study on the cold-rolling effects on mechanical and microstructural characteristics of commercial pure aluminum up to the large strains. Likewise, the influence of post-rolling on the nature and behavior of SPDed materials have been studied scarcely. Attention has been focused on steels, copper, aluminum, magnesium, titanium and their alloys [15,19–22]. It was ascertained that exertion of subsequent rolling on SPDed matter could accelerate the grain refinement and improve the material strength. Beside, often it has been reported that this enhancement was attended by drop in ductility [21]. Of course, carry on rolling to the elevated strains exclusively might break the material's resistance due to micro-cracks propagation since their formation is elucidated to be inevitable in such large deformations. This threat is contingent when the archetypal has a thickness within low range scales.

Despite of the investigation into the cold-rolling influence on some SPDed alloys, regardless of the type of alloy and the utilized method, no render has been reported previously about the lattice transformation while rolling as the terminal processing of CGPed materials. Briefly explained reasons beside profuse unanswered questions about the rolling-direction effects on microstructural and mechanical characteristics of already strained aluminum alloys by CGP method was motivated the authors to inquire the correlation of lattice parameters and achieved material properties for Al-Mn-Si alloy in hypothesized deformation paths.

2. Materials and methods

Pieces with 84 mm × 70 mm × 3 mm dimensions were cut and prepared from Al-Mn-Si sheet which was pre-annealed at 723 K for 3 h in order to survey the impact of CGP and subsequent rolling processes. Fig. 1 illustrates the corrugating and flattening CGP dies used in the present study.

The width of dents in corrugating dies was identical to sheet thickness which lead to impose highly-pure shear stress while processing. The pressing force was supplied via a 100 kN hydraulic pressing machine equipped with a digital force-meter with constant ram displacement speed of 0.1 mm s^{-1}. The applied pressing load was 45–50 kN which was around 45–50% of nominal machine capacity. In order to extenuate the tangible friction between the processing die and specimens, Teflon tape as lubricant wrapped around the aluminum sheets rigorously. Already, analysis of force diagrams was revealed that friction could have ascertained influence on the deformation force [23].

In the following, two-pass CGPed Al-Mn-Si specimens were direct- and cross-rolled at room temperature by the strains of 0.47, 0.8 and 1.27. A laboratory 200 kN rolling machine with cylindrical rolls (ϕ = 150 mm) and feeding speed of 30 rpm was utilized. Comparing the primary and final sheet thicknesses,

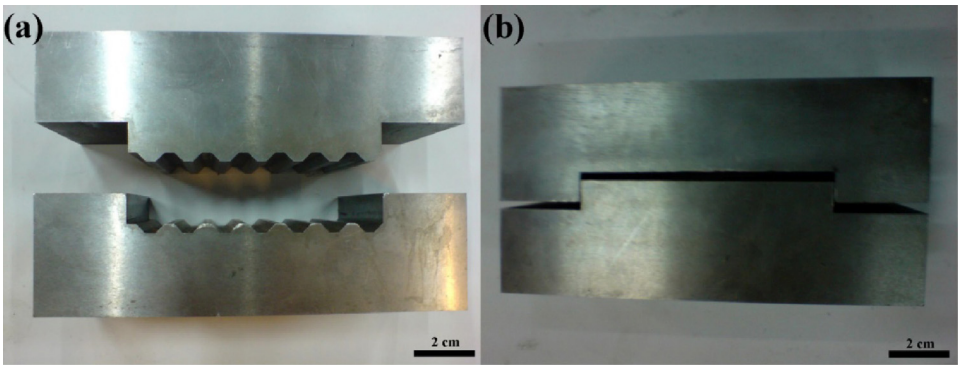

Fig. 1 – Illustration of (a) corrugated and (b) flattened dies applied in CGP process.

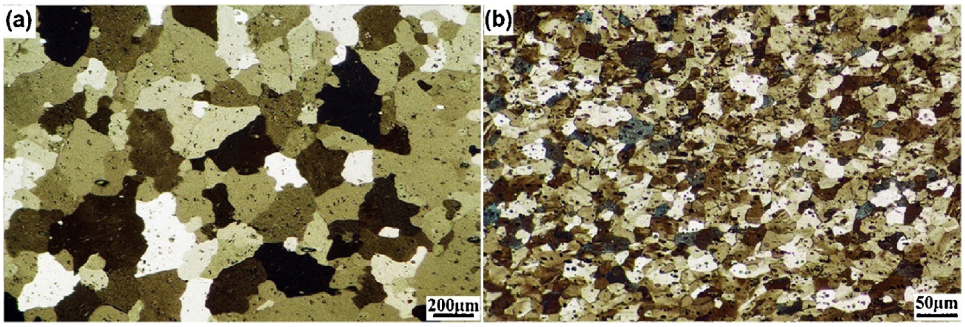

Fig. 2 – Optical micrographs depict the microstructure of the (a) annealed and (b) two-pass CGPed Al-Mn-Si sheets.

the reductions were appreciable enough since the fluctuations of thickness were in the range of 6–10%. Direct-rolling was carried out along longitudinal direction of CGPed sheet while the cross-rolling was performed by a 90° clockwise rotation.

To investigate the lattice evolutions, X-ray diffraction (XRD) analysis were carried out using a Philips X-ray diffractometer equipped with a graphite monochromator using CuKα radiation. The X-ray patterns of the samples were acquired in the range of 30°–80° and step width of 0.02°. For calibration of the instrumental line broadening, SiC powder was examined in the same condition. Resolving full-width at half-maximum (FWHM) for all peaks was carried out using the software configured with the XRD system. Williamson–Hall method as a reliable approach for analysis of X-ray diffraction was utilized in this study [24,25]. Accordingly, crystallite size and lattice equivalent strain calculated using the deviation of line profile from the perfect crystal diffraction.

Microstructure of the samples along the rolling direction (RD) was investigated after anodic oxidation applying JE-WorldTech [9,10] patented reagent and using cross polarizers. The initial average grain/crystallite size of pre-annealed Al-Mn-Si sheet was 730 nm. Meanwhile, to investigate the mechanical behavior of specimens, room temperature tension and hardness tests were performed in both applied directions. Tensile samples were run in a machine according to ASTM E8M standard and the tests were performed using an Instron machine at strain rate of $2 \times 10^{-4}\,s^{-1}$. Vickers hardness measurements were carried out using a 5 kg load for 30 s as dwelling time. The hardness values were reported from the average of discrete measurements for each specimen.

3. Results and discussion

3.1. *Microstructure*

The microstructure of pre-annealed Al-Mn-Si sheets contained large equiaxed grains (Fig. 2(a)). Fig. 2(b) presented the evidence of grain refinement and shearing after imposing the second CGP pass.

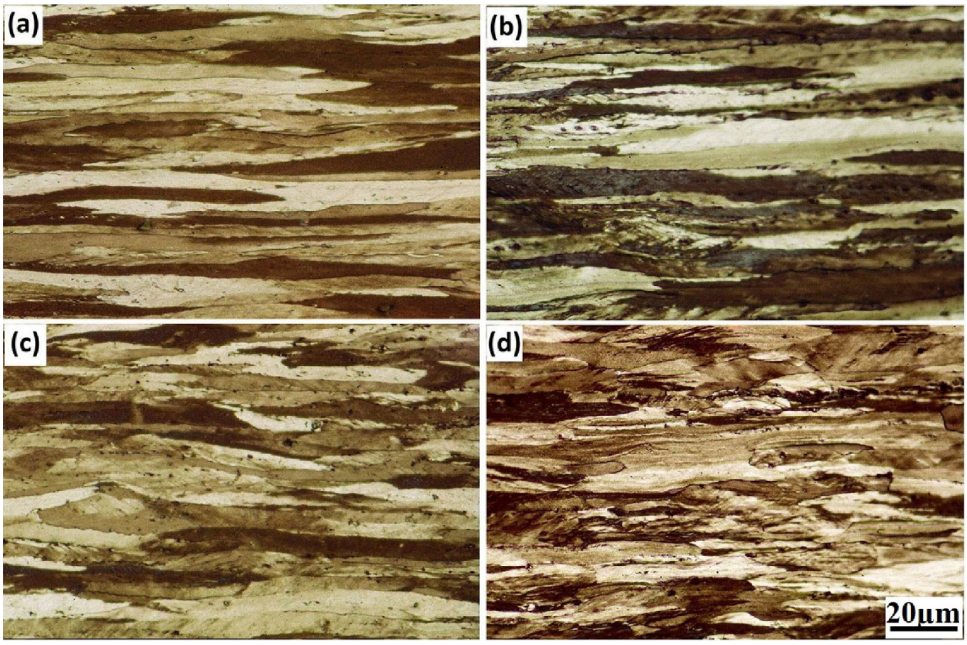

Fig. 3 – Optical micrographs showing lamellar microstructures of rolled Al-Mn-Si with 1.27 strain after (a) direct-rolling of annealed specimen, (b) direct-rolling of two-pass CGPed specimen, (c) cross-rolling of annealed specimen and (d) cross-rolling of two-pass CGPed specimen.

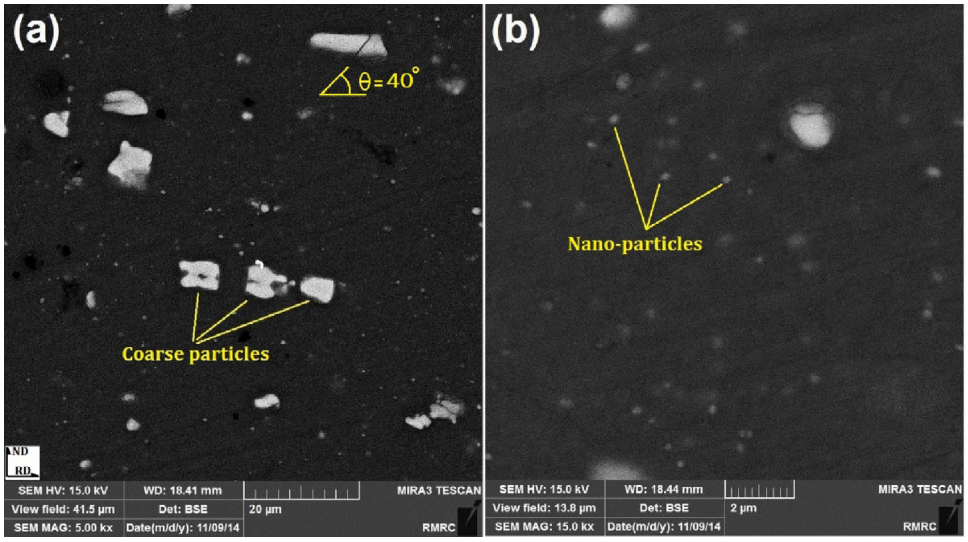

Fig. 4 – Back scatter FESEM micrograph of intermetallic particles distribution in longitudinal cross-section of rolled CGPed alloy illustrating (a) coarse particles and (b) nanoparticles.

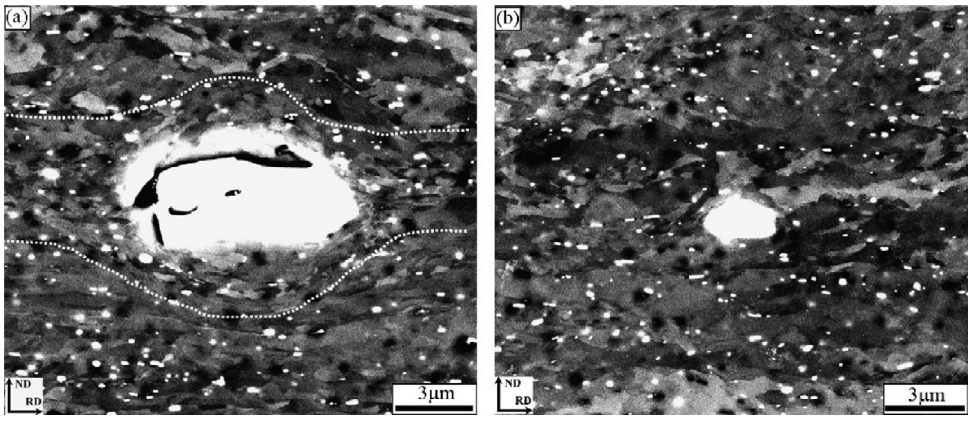

Fig. 5 – Example of deformed microstructures showing the influence of constituent AlFeMnSi particle size at 70% reduction: (a) obvious deformation zones around large particles; (b) no deformation zones around small particles and dispersoids [28].

The optical micrographs of rolled and rolled + CGPed Al-Mn-Si sheets in different rolling directions are shown separately in Fig. 3.

In both deformation routes, lamellar structures were obtained; however, post-rolling of two-pass CGPed sheets resulted in finer elongated grains due to primary refining through CGP. Results are also validated with whatever reported by Stepanov et al. for ECAPed specimens after post-rolling [12]. Structural uniformity enhancement in pre-deformed samples after subjection to cold rolling rationalized on the fact that CGP solely have potential of non-uniformity extension within microstructure apart from grain refinement. Beside, existed intermetallic particles within matrix could toughen up microstructure non-uniformity. As shown in Fig. 4, intermetallics could be categorized in size within two classes included coarse and nano dispersed particles.

Deformation of alloy containing large non-deformable particles leads to incompatibilities creation at matrix/particle interfaces and formation of so-called deformation zones around the particles [26,27]. Large lattice rotations, which can be associated with the operation of the active slip systems, have been found in the deformation zones around such particles. EDS elemental analysis results suggested that most of the intermetallic particles have chemical arrays consisted of Al_6Mn, AlFeMnSi and Al_4MnSi. This was evident from Fig. 4(b) that most of the fine dispersoids were smaller than 200 nm. On the other side, coarse particles were in the range of 2–12 μm with average length of 7.5 μm. Slight distortion of grain boundaries aligned along the rolling direction is occasionally observed in grains containing the coarse particles (Fig. 5(a)).

While based on literature [28–32], randomly distributed nanoparticles in matrix have negligible effect on the general characteristics of the deformation flow in microstructure (Fig. 5(b)). However, they have undeniable effect on microstructure stabilizing by pinning dislocation, grains and sub-grains boundaries [33]. High strains create large scale structural heterogeneities in the form of deformation zones around the large particles which are elongated in the rolling

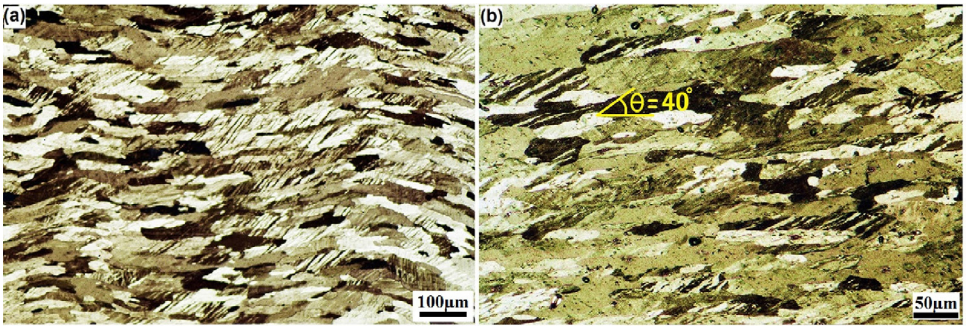

Fig. 6 – Micro-shear bands in longitudinal cross-section of rolled CGPed Al-Mn-Si sheets (a) cluster of grains and (b) individual grains.

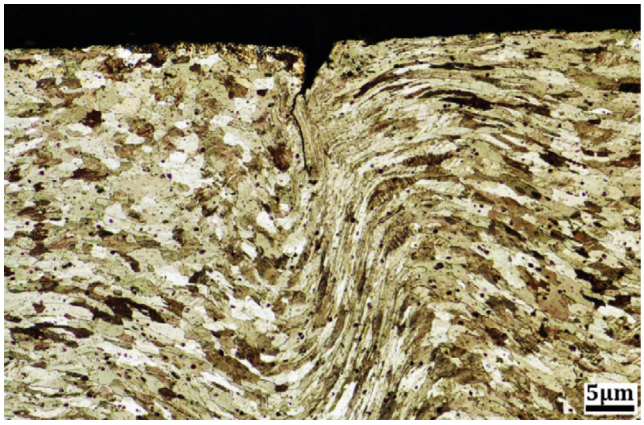

Fig. 7 – Optical micrograph showing the micro-crack formation at aluminum sheet surface after subjection to four passes of CGP [10].

direction. The coarse particles play a critical role in stress localization around themselves, leading to the formation of well-defined deformation zones. At these locations highly misoriented regions containing significant orientation gradients are developed with the maximum misorientations occurring near coarser particles [28]. Coarse particles would give up against work-hardening and dislocations aggregation around themselves and fragment into smaller pieces along the applied shear stress (Fig. 4(a)). Fig. 6 alludes to the fact that rolling of CGPed Al-Mn-Si samples by 0.47 strains had developed micro-shear bands within some grains aligned ~40° to the RD.

Similar observations was reported by Liu et al. [28] and Lens et al. [34] on Al-Mn alloys formerly. The response for shear-bands' formation at some particular locations within UFG materials has not been underpinned by the same mechanism rigorously. Indeed, micro-shear bands' generation in structure would due to non-uniform strain distribution inside deformed samples. Partial work-hardening in strain localized zones would be dragged to a saturated level break the lattice perseverance and lead to grains dividing. Jia et al. [35] proposed that shear-bands initiated from the large soft grains and higher stress-concentrated locations. In the following, they could be extended by the rotation of cluster of grains (Fig. 6(a)) or individual grains (Fig. 6(b)). This would even result in the premature fracture of the sample while deformation (Fig. 7).

As shown, shear-band formation in crushed zone under surface micro-crack facilitates the crack growth through the severely work-hardened region. The micro-shear banding provides paths by which the extensive operation of slip systems and high dislocation density promote the initiation of DRX followed by reorientation of basal planes parallel to the shear plane [36].

After rolling of CGPed sheets by desired strain, the microstructure evolved into a layered structure containing lamellar boundaries aligned along the RD. This finding favored the reported results for SPDed commercial pure aluminum undergone cold-rolling by heavy strains [20,21,37,38]. From Fig. 8, obviously the lamellar boundary spacing was decreased, the laminate structure became more compressed and grains got more elongated along the RD upon the rolling strain increased either in direct or cross direction [37,38].

According to Fig. 8(a) and (d), at low strain levels, evidently cross-rolling had more distinction to direct-rolling with respect to generated narrower and finer grains. While direct-rolling had more contribution at the moderate to high rolling strains.

3.2. *X-ray diffraction pattern analysis*

Williamson–Hall method was utilized to calculate crystallite size, dislocation density and lattice equivalent strain. Based on the correlation between full-width at half-maximum and peak intensity (β), crystallite size (t) and the distortion function ($f(\varepsilon)$) [25,39], following equation could be applied [25]:

$$\beta\cos\theta = \frac{k\lambda}{t} + f(\epsilon)\sin\theta \tag{1}$$

where θ is the Bragg angle, λ is the wavelength and k is the Scherer's constant (≈0.9). The intercept of the plotted $\beta\cos\theta$ versus $\sin\theta$ gave the crystallite size while the slope gave the crystal strain. As commercial diffractometers contain the instrumental profile beside the intrinsic profile (pure diffraction profile), the Gaussian–Gaussian function could be employed to correct the integral breadths of intrinsic profile [25] as follows:

$$\beta^2_{\exp} \cong \beta^2 + \beta^2_{ins} \tag{2}$$

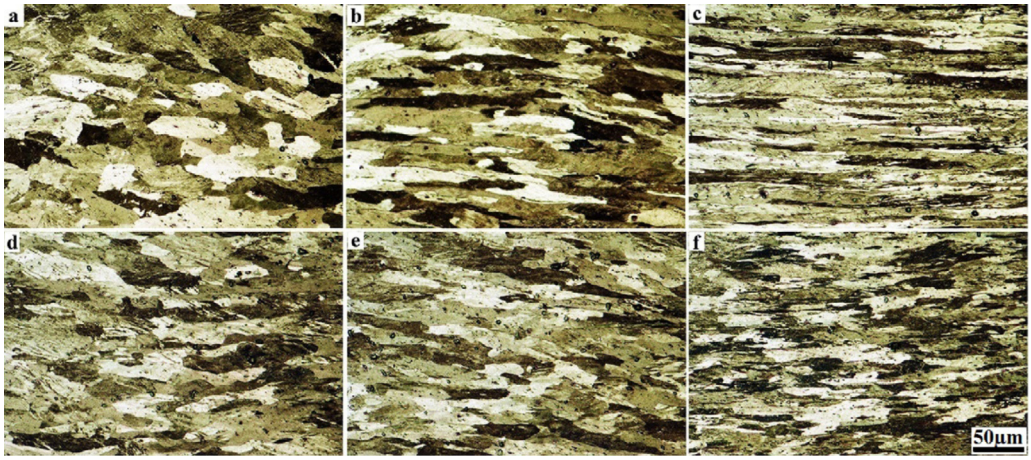

Fig. 8 – The microstructure of two-pass CGPed Al-Mn-Si sheets with subsequent straining of: (a) 0.47 direct-rolling, (b) 0.8 direct-rolling, (c) 1.27 direct-rolling, (d) 0.47 cross-rolling, (e) 0.8 cross-rolling and (f) 1.27 cross-rolling.

where β, β_{exp} and β_{ins} are the integral breadth of the intrinsic, experimental and instrumental profiles, respectively. The value of the dislocation density (ρ) was calculated from the average values of the crystallite size (D) and micro-strain (ε_L) as follows [40,41]:

$$\rho = \sqrt{\rho_D \times \rho_S} \tag{3}$$

$$\rho_D = \frac{3}{D} \tag{4}$$

$$\rho_s = \frac{K\langle \epsilon_L^2 \rangle}{b^2} \tag{5}$$

where $K = 6\pi$ and b is the Burger's vector ($b = a/\sqrt{2}$ for FCC materials since a is the lattice parameter which could be considered equal to 4.097 Å for aluminum).

During severe plastic deformation, sub-grain boundaries evolve within the grains/crystallite structure [42]. Subsequently, boundaries develop areas with coherent crystalline domain size [12]. Lattice transitions during CGP, rolling and post-rolling of CGPed Al-Mn-Si alloy was ascertained by analyzing the XRD patterns. Crystallite size variation as a function of imposed strain during CGP and rolling is sketched in Fig. 9. It is obvious that the first pass of CGP was the most effective pass on grain refinement and subsequent passes have not had any worthwhile advantages [10]. This is completely in accordance with previous reported results on CGP [43,44]. While the rolling traced more prominent footprint compared to CGP and the first rolling reduction led to drastic reduction of the crystallite size. Further straining through rolling was followed by the crystallites' growth.

Changes of dislocation density in annealed Al-Mn-Si sheet during subjection to CGP and rolling is plotted in Fig. 9.

Comparing Figs. 9 and 10, showed that cold rolling imposed heavy effective strain to the extent that dislocation density attained a saturate level after the first reduction.

Carry on rolling led to dislocation annihilation through DRX in crowded areas. So, increasing the rolling strain beyond the 0.8 resulted in large drop in dislocations density and growth of crystallites. On the other side, distinctly the latter passes of CGP had inconsequential effect on grain refinement and it was fair to conclude that CGP would not be capable to approach the nanoscale grain size. According to Fig. 10, imposed strain plays an essential role on dislocations accumulation and closed them to the noted saturation limit. Pouraliakbar et al. [10] reported that severe straining through CGP can be accompanied by surface micro-cracks formation in deformed sheet before DRX start (Fig. 8) and prevent from dislocation density to exceed from a certain value.

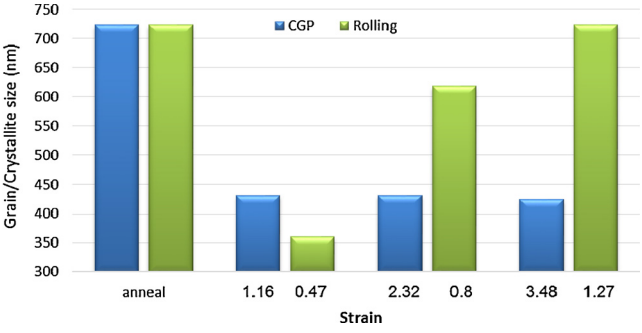

Fig. 9 – The effect of CGP and rolling strain on grain/crystallite size of pre-annealed Al-Mn-Si sheet.

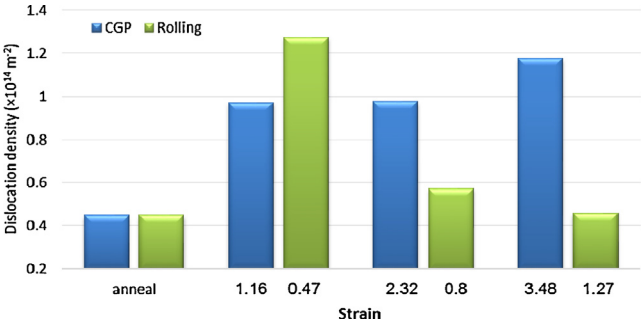

Fig. 10 – The effect of CGP and rolling strain on dislocation density of pre-annealed Al-Mn-Si sheet.

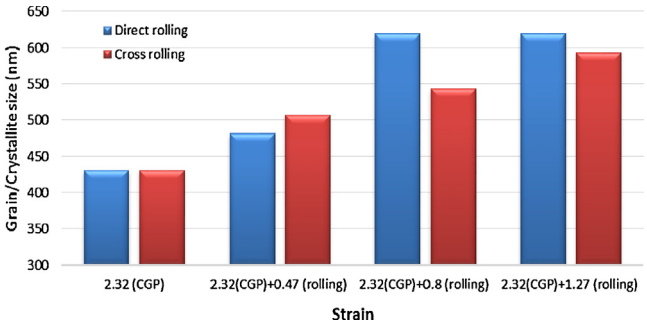

Fig. 11 – The effect of direct- and cross-rolling strain on grain/crystallite size of two-pass CGPed Al-Mn-Si alloy.

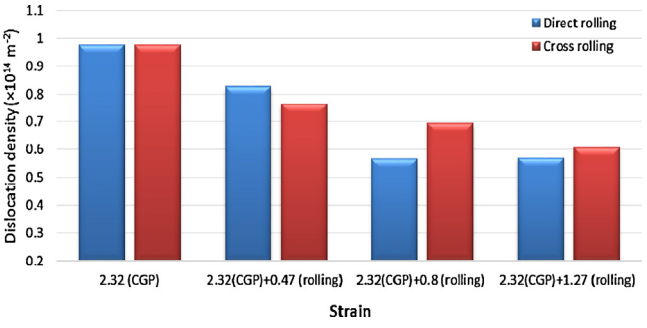

Fig. 12 – The effect of direct- and cross-rolling strain on dislocation density of two-pass CGPed Al-Mn-Si alloy.

Impact of direct- and cross-rolling on crystallite size variation of two-pass CGPed specimen could be observed in Fig. 11.

As shown, the average grain size was reduced from 723 nm in annealed state to 431 nm after second pass of CGP. Such a similar trend was also reported by Krishnaiah et al. [43] for commercial aluminum undergone CGP process. As it was expected, crystallites began to growth upon the post-rolling start. Difference in maximum achieved grain size after direct- (619 nm) and cross-rolling (593 nm) could be associated with different structural texture formed via deformation routes. Additionally, tracing the slope of the grain size variation revealed that grain coarsening had taken place by the same rate in cross-rolled specimens while DRX had happened more intensive through direct-rolling. In lower rolling strains, the crystallite size of cross-rolled CGPed aluminum was coarser than that for direct-rolled one. But, higher rolling strains inversed the results. Likewise, optical metallographic observations qualitatively supported the obtaind results by XRD.

It has been recognized that dislocation density could be calculated as a function of rolling strain [25]. Fig. 12 shows the dislocation density variations for two-pass CGPed specimens followed by direct- and cross-rolling.

Noticeably from Fig. 9, CGP before applying post-rolling to Al-Mn-Si sheets had increased the dislocation density from 0.45×10^{14} to 0.977×10^{14} m^{-2} since the first rolling reduction with 0.47 strain was raised this amount to a saturate level of 1.276×10^{14} m^{-2}.

From Fig. 12, merging the CGP and rolling had followed two main advantages. The first was that, regardless of rolling direction, per-straining via CGP triggered the crystallites growth upon the post-rolling start. The second was that direct-rolling was more impressive on dislocation accumulation and grain coarsening owing to dislocation annihilation during DRX. Direct-rolling not only created outnumber dislocations and consequentially coarser recrystallized grains, but also seized higher dislocation generation rate and sooner reached to an optimum value. Also, rolling of CGPed Al-Mn-Si sheet encountered with reduction in slope of dislocation annihilation compared to cold rolling of annealed specimen and increased the dislocation density after 1.27 rolling strain from 0.457×10^{14} m^{-2} for just rolled sample to 0.57×10^{14} m^{-2} and 0.607×10^{14} m^{-2} for direct- and cross-rolled CGPed specimens, respectively. Obtained trends for crystallite size and dislocation density variation (Figs. 11 and 12) were completely in contrast with former results on rolled CGPed AA1100 [45]. Dislocations value and arrangement could affect other mechanical characteristics of specimen.

Fig. 13 demonstrates the XRD patterns acquired from rolled Al-Mn-Si specimens and Table 1 lists the peak intensity ratio for (111), (200), (220) and (311) crystallographic planes.

Accordingly, maximum intensity in annealed specimen was related to (200) plane (Fig. 13(a)). By two passes of CGP, (111) and (200) slip planes were significantly consolidated and these were accompanied by decline in (220) peak intensity. This result can be attributed to intrinsically shear extender

Table 1 – The intensity ratios of crystallographic planes in direct- and cross-rolled Al-Mn-Si specimens processed under different conditions.

Series	CGP pass	Rolling direction	Rolling strain	Peak intensity ratio (I/I_{max})			
				(111)	(200)	(220)	(311)
1	0	–	0	32	32	**100**	60
2	2	–	0	**100**	99	61	62
3	0	Longitudinal	0.8	55	24	**100**	82
4	0	Cross	0.8	33	52	**100**	63
5	2	Longitudinal	0.47	52	**100**	60	57
6	2	Longitudinal	0.8	**100**	78	65	70
7	2	Longitudinal	1.27	40	46	**100**	84
8	2	Cross	0.47	93	88	**100**	62
9	2	Cross	0.8	54	47	**100**	55
10	2	Cross	1.27	44	36	**100**	62

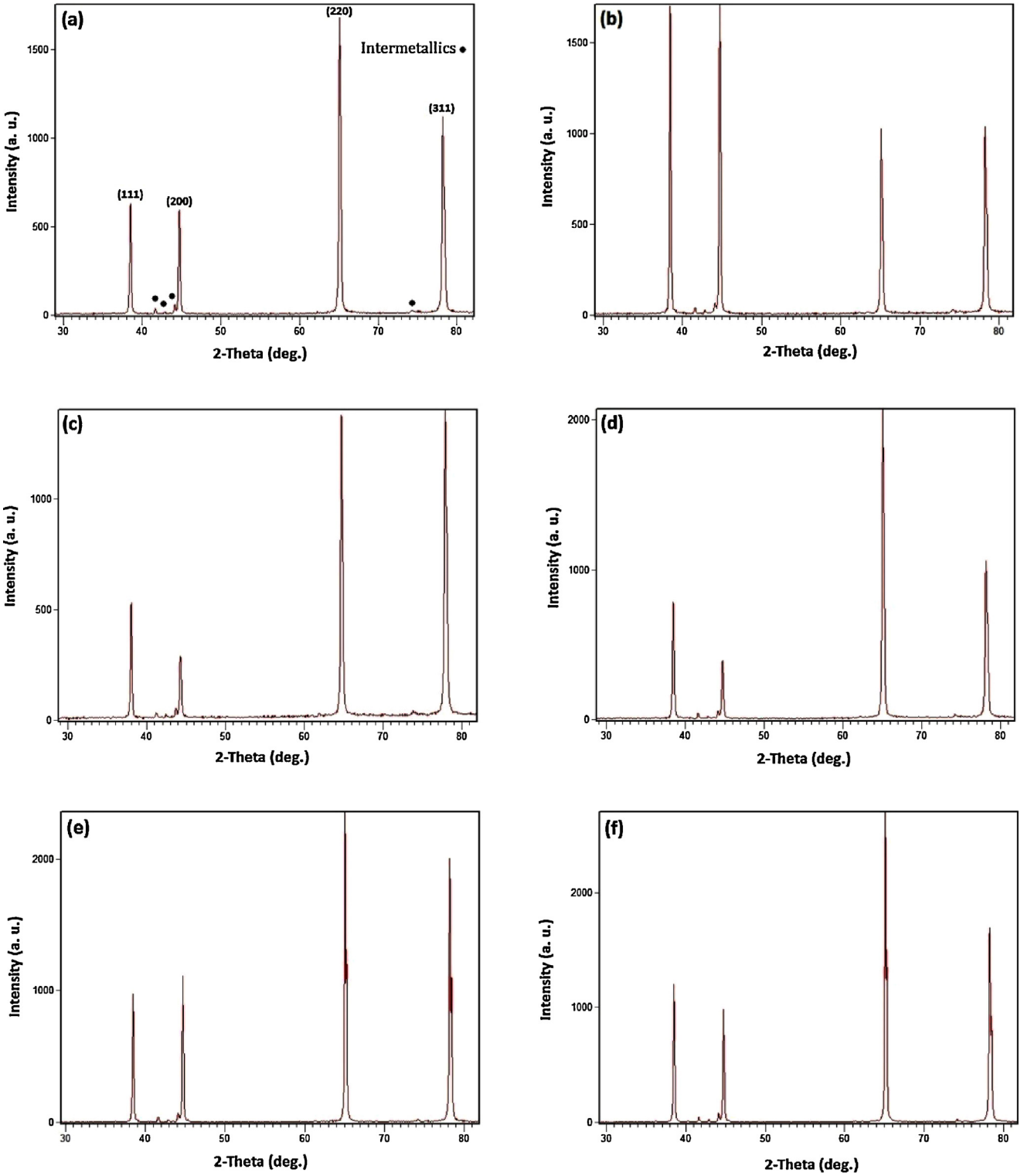

Fig. 13 – XRD patterns of Al-Mn-Si specimens under different processing conditions of (a) annealed, (b) two-pass CGPed, (c) direct-rolled with 1.27 strain, (d) cross-rolled with 1.27 strain, (e) direct-rolling of two-pass CGPed with 1.27 strain and (f) cross-rolling of two-pass CGPed with 1.27 strain.

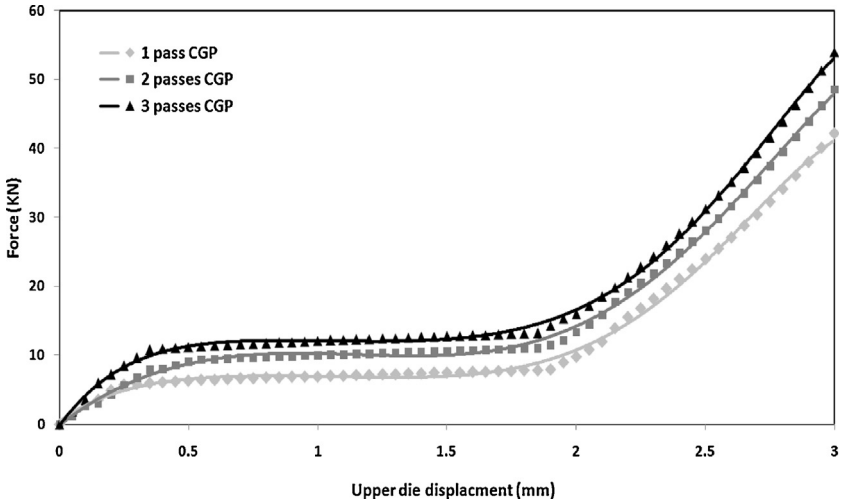

Fig. 14 – Examined force-displacement graphs for first, second and third passes of CGP.

nature of CGP process evidenced by amplification of (111) plane as slip plane of FCC metals [46,47]. Rolling of annealed specimen had negligible effect on peak intensity ratios and almost pre-processing observed trends remained unchanged at the end of direct- and cross-rolling. Of course, direct-rolling was more impressive on (311) peak augmentation. The gradual grain size decrement during consecutive passes of CGP could be also surmised from the peaks' broadening in XRD pattern [36].

According to Table 1, post-rolling of CGPed specimen changed the crystallographic characteristics and led to ennoblement of peak intensity ratio for (220) plane.

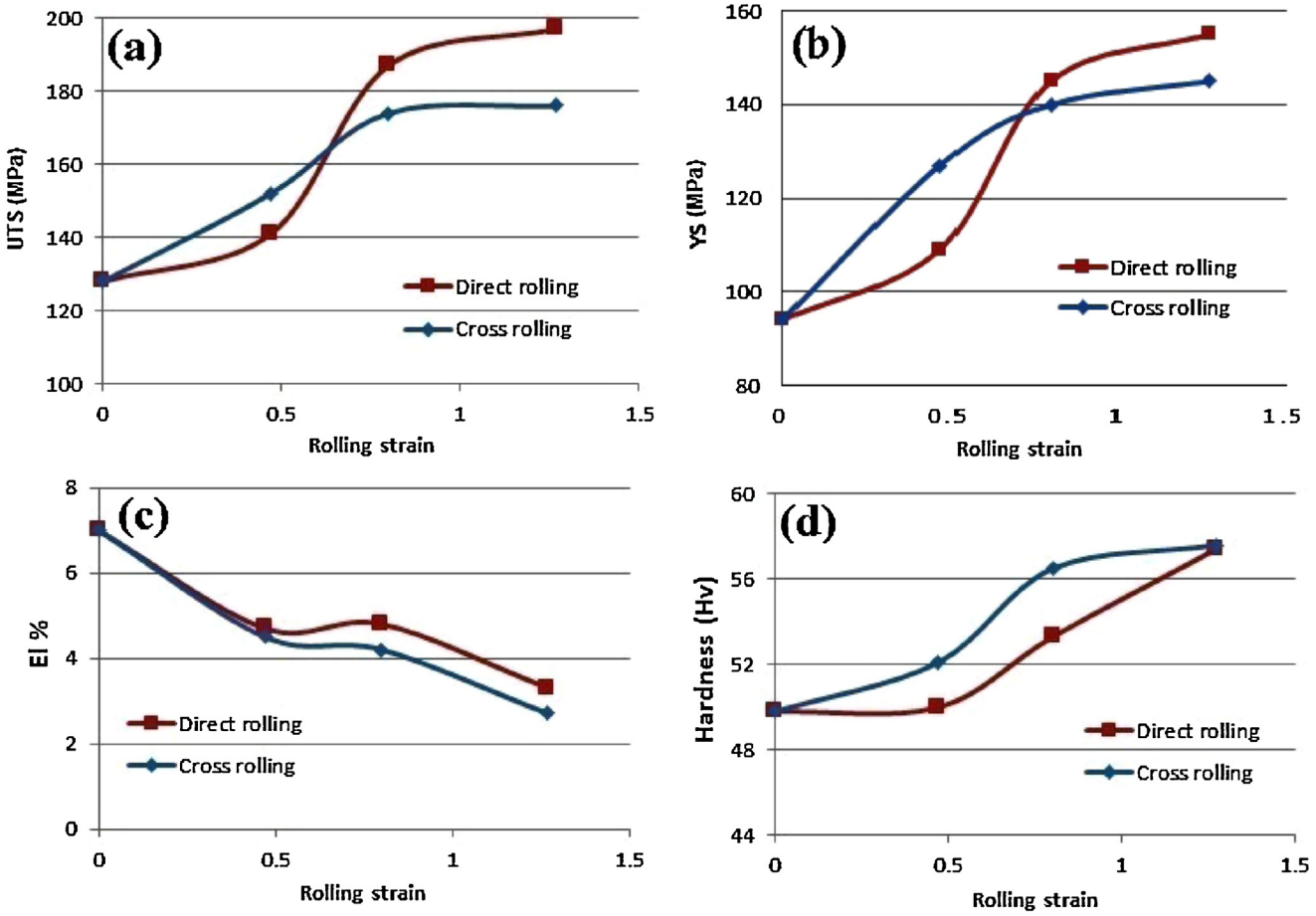

Fig. 15 – The variation of mechanical properties of CGPed Al-Mn-Si with subsequent rolling in different directions: (a) UTS, (b) YS, (c) elongation and (d) hardness.

For two-pass CGPed specimen which followed by 0.8 direct-rolling strain, obviously the (111) planes had the maximum intensity ratio. But, XRD pattern of cross-rolled samples rationalized on that CGPed sheets were insensitive to increasing the rolling strain in cross direction. This was accommodated to rolling effect on archetypal in which drastic decline in the rolling reduction enhanced the (200) intensity ratio in rolled specimens. This contradiction in crystallographic characteristics owing from fundamental difference between deformation paths of CGP and rolling. Increasing the rolling strain, changed the (111) to (220) as for rolled CGPed specimens. This trend revealed that the preferred plane orientation of post-rolled samples was (220). Observed trends for peak intensity ratios in Fig. 13(e) and (f) was in agreement with crystallite size and dislocation density variations during direct- and cross-rolling of CGPed sheets (Figs. 11 and 12). As can be seen, the rolling contribution overcome on CGP and lead to (220) and (311) peaks intensification; since CGP had boosting effect on (111) and (200) peaks. Furthermore, direct-rolling was more effective compared to cross-rolling, especially on (311) plane reinforcement.

3.3. *Mechanical properties*

Fig. 14 illustrates the experimental force-displacement graph variation during the consecutive passes of CGP.

Based on figure, force fluctuation trend in each graph could be sub-divided into three different zones; however, increase in pass number had undeniable effect on the applied force due to the flow stress enhancement in already deformed material. At the first stage, the appreciable incline of the curve raised from the shear strain localization around the grooved areas. In the following, forming force was increased gradually accommodated with the upper die displacement. This was due to the propagation of plastic deformation and development of flow stress within these regions. At the latter step, the remarkable addition to applied force was resulted from contact surface extension between the specimen and die appended the further friction. The flow stress demonstrated an upward trend up to the third pass of CGP.

Fig. 15 shows the effect of post-rolling strain on hardness and tensile characteristics of CGPed Al-Mn-Si alloy.

The UTS and YS of the specimens were enhanced while ductility was decreased with increasing the rolling strain. The substantial changes were appeared in YS and elongation values. Not any distinctive decrease was observed in mechanical properties of rolled CGPed specimens even after rolling with higher strains. Maximum tensile strength was achieved after direct-rolling of CGPed Al-Mn-Si specimen with 1.27 rolling strain according to 197 MPa, 155 MPa and 3% reported values for UTS, YS and elongation, respectively. By comparison of obtained results for UTS and YS of CGPed samples, it could be concluded that the role of direct-direction was more highlight on mechanical properties' enhancement at higher rolling strain. This could be associated with the effect of deformation path on microstructural evolutions and crystallographic preferences. After post-rolling of two-pass CGPed aluminum with 1.27 rolling strain, the UTS was evolved to 197 MPa for direct-rolling and 176 MPa for cross-rolling which was 100% greater than initial strength (98 MPa). Rahimi Mamaghani et al. [45] reported inverse mechanical results compared to present outputs and announced the cross-rolling as the effective deformation route on strength enhancement of CGPed AA1100. Despite of better performance of direct-rolling on tensile strength enhancement, hardness was not affected significantly by rolling direction. Comparison of mechanical results by X-ray outputs indicated that at lower rolling strain (up to 0.47) cross-rolling of CGPed sheets had more influence on dislocation accumulation followed by mechanical properties improvement compared to direct one since post-rolling by higher strains reversed the results.

4. Conclusions

Rolling the CGPed Al-Mn-Si specimens as supplementary deformation process was successfully executed up to severe strains. Compact lamellar structure contained elongated grains was achieved by increasing the rolling strain. Using rolling as post processing on CGPed sheets accelerated the microstructural refinement. Additionally, analogy of cross- and direct-rolling pointed to higher dislocation accumulation due to rolling of CGPed Al-Mn-Si alloy accompanied by dynamic recrystallization. The minimum crystallite size of 431 nm which was achieved by second pass of CGP was increased to 619 nm and 593 nm through direct- and cross-rolling by 1.27 strain, respectively. Based on XRD patterns, it was concluded that post-rolling had not distinctive effect on peaks' pattern and (200) planes preserved the maximum intensity ratios in rolled specimens as for annealed one; however, CGP changed the pattern in such a way that (111) had the maximum intensity ratio. Post-rolling of CGPed specimen changed the material's crystallographic characteristics since intensity ratios for (220) plane enhanced. Characteristic peaks in both direct and cross directions were insensitive in confronting with the rolling strain increment. Changing the rolling direction had not any significant effect on microstructural and mechanical characteristics of annealed Al-Mn-Si specimens since the direct-rolling of CGPed aluminum led to improved mechanical properties and finer microstructure compared to those achieved through cross-rolling.

Acknowledgements

The authors gratefully acknowledge the research board of Department of Materials Science and Engineering of *Sharif University of Technology* for the provision of some parts of facilities used in this research. Authors would also like to appreciate Dr. Ali Nazari from *Swinburne University of Technology* for his valuable discussions. Meanwhile, strong supports and persuasions from Dr. Mohsen Kazeminezhad will not be forgotten.

REFERENCES

[1] S. Valipour, A. Eivani, H. Jafarian, S. Seyedein, M. Aboutalebi, Effect of pre-deformation thermomechanical processing on the development of ultrafine grain structure during equal

channel angular extrusion, Materials & Design 89 (2016) 377–384.
[2] M.Y. Murashkin, I. Sabirov, A. Medvedev, N. Enikeev, W. Lefebvre, R. Valiev, et al., Mechanical and electrical properties of an ultrafine grained Al – 8.5 wt.% RE (RE = 5.4 wt.% Ce, 3.1 wt.% La) alloy processed by severe plastic deformation, Materials & Design 90 (2016) 433–442.
[3] R. Luri, J. Fuertes, C. Luis, D. Salcedo, I. Puertas, J. León, Experimental modelling of critical damage obtained in Al-Mg and Al-Mn alloys for both annealed state and previously deformed by ECAP, Materials & Design 90 (2016) 881–890.
[4] K. Edalati, Z. Horita, A review on high-pressure torsion (HPT) from 1935 to 1988, Materials Science and Engineering: A 652 (2016) 325–352.
[5] N. Haghdadi, A. Zarei-Hanzaki, H. Abedi, D. Abou-Ras, M. Kawasaki, A. Zhilyaev, Evolution of microstructure and mechanical properties in a hypoeutectic Al-Si-Mg alloy processed by accumulative back extrusion, Materials Science and Engineering: A 651 (2016) 269–279.
[6] D. Jafarlou, E. Zalnezhad, M. Hassan, M. Ezazi, N. Mardi, A. Hamouda, et al., Severe plastic deformation of tubular AA 6061 via equal channel angular pressing, Materials & Design 90 (2016) 1124–1135.
[7] M. Ruppert, C. Schunk, D. Hausmann, H.W. Höppel, M. Göken, Global and local strain rate sensitivity of bimodal Al-laminates produced by accumulative roll bonding, Acta Materialia 103 (2016) 643–650.
[8] N. Thangapandian, S.B. Prabu, K. Padmanabhan, Effects of die profile on grain refinement in Al-Mg alloy processed by repetitive corrugation and straightening, Materials Science and Engineering: A 649 (2016) 229–238.
[9] M.R. Jandaghi, H. Pouraliakbar, M.K.G. Shiran, G. Khalaj, M. Shirazi, On the effect of non-isothermal annealing and multi-directional forging on the microstructural evolutions and correlated mechanical and electrical characteristics of hot-deformed Al-Mg alloy, Materials Science and Engineering: A (2016).
[10] H. Pouraliakbar, S. Firooz, M.R. Jandaghi, G. Khalaj, A. Amirafshar, Combined effect of heat treatment and rolling on pre-strained and SPDed aluminum sheet, Materials Science and Engineering: A 612 (2014) 371–379.
[11] H. Pouraliakbar, S. Firooz, M.R. Jandaghi, G. Khalaj, A. Nazari, Predicting the ultimate grain size of aluminum sheets undergone constrained groove pressing, The International Journal of Advanced Manufacturing Technology (2016) 1–20.
[12] R.Z. Valiev, R.K. Islamgaliev, I.V. Alexandrov, Bulk nanostructured materials from severe plastic deformation, Progress in Materials Science 45 (2000) 103–189.
[13] I. Nikulin, R. Kaibyshev, T. Sakai, Superplasticity in a 7055 aluminum alloy processed by ECAE and subsequent isothermal rolling, Materials Science and Engineering: A 407 (2005) 62–70.
[14] K.-T. Park, H.-J. Lee, C.S. Lee, D.H. Shin, Effect of post-rolling after ECAP on deformation behavior of ECAPed commercial Al-Mg alloy at 723 K, Materials Science and Engineering: A 393 (2005) 118–124.
[15] H. Akamatsu, T. Fujinami, Z. Horita, T.G. Langdon, Influence of rolling on the superplastic behavior of an Al-Mg-Sc alloy after ECAP, Scripta Materialia 44 (2001) 759–764.
[16] O. Mishin, A. Godfrey, D.J. Jensen, N. Hansen, Recovery and recrystallization in commercial purity aluminum cold rolled to an ultrahigh strain, Acta Materialia 61 (2013) 5354–5364.
[17] T. Yu, N. Hansen, X. Huang, Linking recovery and recrystallization through triple junction motion in aluminum cold rolled to a large strain, Acta Materialia 61 (2013) 6577–6586.
[18] Q. Liu, X. Huang, D. Lloyd, N. Hansen, Microstructure and strength of commercial purity aluminium (AA 1200) cold-rolled to large strains, Acta Materialia 50 (2002) 3789–3802.
[19] S.S. Hazra, A.A. Gazder, A. Carman, E.V. Pereloma, Effect of cold rolling on as – ECAP interstitial free steel, Metallurgical and Materials Transactions A 42 (2011) 1334–1348.
[20] V.V. Stolyarov, Y.T. Zhu, I.V. Alexandrov, T.C. Lowe, R.Z. Valiev, Grain refinement and properties of pure Ti processed by warm ECAP and cold rolling, Materials Science and Engineering: A 343 (2003) 43–50.
[21] K.-T. Park, H.-J. Lee, C.S. Lee, W.J. Nam, D.H. Shin, Enhancement of high strain rate superplastic elongation of a modified 5154 Al by subsequent rolling after equal channel angular pressing, Scripta Materialia 51 (2004) 479–483.
[22] O. Antonova, A.Y. Volkov, B. Kamenetskii, D. Komkova, Microstructure and mechanical properties of thin magnesium plates and foils obtained by lateral extrusion and rolling at room temperature, Materials Science and Engineering: A 651 (2016) 8–17.
[23] A. Shirdel, A. Khajeh, M. Moshksar, Experimental and finite element investigation of semi-constrained groove pressing process, Materials & Design 31 (2010) 946–950.
[24] M.R. Rezaei, M.R. Toroghinejad, F. Ashrafizadeh, Production of nano-grained structure in 6061 aluminum alloy strip by accumulative roll bonding, Materials Science and Engineering: A 529 (2011) 442–446.
[25] Z. Zhang, F. Zhou, E. Lavernia, On the analysis of grain size in bulk nanocrystalline materials via X-ray diffraction, Metallurgical and Materials Transactions A 34 (2003) 1349–1355.
[26] F. Humphreys, The nucleation of recrystallization at second phase particles in deformed aluminium, Acta Metallurgica 25 (1977) 1323–1344.
[27] F. Humphreys, Local lattice rotations at second phase particles in deformed metals, Acta Metallurgica 27 (1979) 1801–1814.
[28] Q. Liu, Z. Yao, A. Godfrey, W. Liu, Effect of particles on microstructural evolution during cold rolling of the aluminum alloy AA3104, Journal of Alloys and Compounds 482 (2009) 264–271.
[29] H. Merchant, J. Morris, D. Hodgson, Characterization of intermetallics in aluminum alloy 3004, Materials Characterization 25 (1990) 339–373.
[30] E. Gomaa, M. Mohsen, A. Taha, M. Mostafa, A study of annealing stages in Al-Mn (3004) alloy after cold rolling using positron annihilation lifetime technique and Vickers microhardness measurements, Materials Science and Engineering: A 362 (2003) 274–279.
[31] S. Chen, N. Kuijpers, S. Van Der Zwaag, Effect of microsegregation and dislocations on the nucleation kinetics of precipitation in aluminium alloy AA3003, Materials Science and Engineering: A 341 (2003) 296–306.
[32] H.-W. Huang, B.-L. Ou, Evolution of precipitation during different homogenization treatments in a 3003 aluminum alloy, Materials & Design 30 (2009) 2685–2692.
[33] M. Komarasamy, R. Mishra, Serration behavior and shear band characteristics during tensile deformation of an ultrafine-grained 5024 Al alloy, Materials Science and Engineering: A 616 (2014) 189–195.
[34] A. Lens, C. Maurice, J. Driver, Grain boundary mobilities during recrystallization of Al-Mn alloys as measured by in situ annealing experiments, Materials Science and Engineering: A 403 (2005) 144–153.
[35] D. Jia, K. Ramesh, E. Ma, Effects of nanocrystalline and ultrafine grain sizes on constitutive behavior and shear bands in iron, Acta Materialia 51 (2003) 3495–3509.
[36] P. Changizian, A. Zarei-Hanzaki, M. Ghambari, A. Imandoust, Flow localization during severe plastic deformation of AZ81 magnesium alloy: micro-shear banding phenomenon, Materials Science and Engineering: A 582 (2013) 8–14.
[37] G. Wu, D. Juul Jensen, Recrystallisation kinetics of aluminium AA1200 cold rolled to true strain of 2, Materials Science and Technology 21 (2005) 1407–1411.

[38] T. Furu, R. Ørsund, E. Nes, Subgrain growth in heavily deformed aluminium—experimental investigation and modelling treatment, Acta Metallurgica et Materialia 43 (1995) 2209–2232.
[39] P. Mukherjee, A. Sarkar, P. Barat, S. Bandyopadhyay, P. Sen, S. Chattopadhyay, et al., Deformation characteristics of rolled zirconium alloys: a study by X-ray diffraction line profile analysis, Acta Materialia 52 (2004) 5687–5696.
[40] P. Sahu, M. De, S. Kajiwara, Microstructural characterization of stress-induced martensites evolved at low temperature in deformed powders of Fe-Mn-C alloys by the Rietveld method, Journal of Alloys and Compounds 346 (2002) 158–169.
[41] H. Pal, A. Chanda, M. De, Characterisation of microstructure of isothermal martensite in Fe-23Ni-3.8 Mn by Rietveld method, Journal of Alloys and Compounds 278 (1998) 209–215.
[42] T. Ungár, The meaning of size obtained from broadened X-ray diffraction peaks, Advanced Engineering Materials 5 (2003) 323–329.
[43] A. Krishnaiah, U. Chakkingal, P. Venugopal, Production of ultrafine grain sizes in aluminium sheets by severe plastic deformation using the technique of groove pressing, Scripta Materialia 52 (2005) 1229–1233.
[44] A. Krishnaiah, U. Chakkingal, P. Venugopal, Applicability of the groove pressing technique for grain refinement in commercial purity copper, Materials Science and Engineering: A 410 (2005) 337–340.
[45] K.R. Mamaghani, M. Kazeminezhad, The effect of direct and cross-rolling on mechanical properties and microstructure of severely deformed aluminum, Journal of Materials Engineering and Performance 23 (2014) 115–124.
[46] J.-C. Lee, H.-K. Seok, J.-H. Han, Y.-H. Chung, Controlling the textures of the metal strips via the continuous confined strip shearing (C2S2) process, Materials Research Bulletin 36 (2001) 997–1004.
[47] G.G. Niranjan, U. Chakkingal, Deep drawability of commercial purity aluminum sheets processed by groove pressing, Journal of Materials Processing Technology 210 (2010) 1511–1516.